Vol. 19, Sup. 1 (2020) 469-481
Revista Mexicana de Ingeniería Química

Corrosion behavior of steel reinforcement bars embedded in concrete with sugar cane bagasse ash

Comportamiento a la corrosión de barras de acero de refuerzo embebidas en concreto con ceniza de bagazo de caña de azúcar

D.E. Ramírez-Arreola[1], F.J. Aranda-García[1], C. Sedano-de la Rosa[1]*, A.M. Camacho-Vidrio[1], R.V. Silva[2]

[1] *Universidad de Guadalajara, Centro Universitario de la Costa Sur, Av. Independencia Nacional 151, Autlán de Navarro, Jalisco, CP 48900, México.*

[2] *CERIS, Instituto Superior Técnico, Universidade de Lisboa, Av. Rovisco Pais, 1049-001 Lisboa, Portugal.*

Received: May 1, 2020; Accepted: June 25, 2020

Abstract

The corrosion behavior of G42 steel reinforcing bars embedded in modified concrete was studied, using cylindrical concrete specimens with sugar cane bagasse ash (SCBA) as partial replacement for Portland cement at proportions of 0, 15, 30 and 45 wt%. The specimens were exposed to a brine environment using the impressed current technique during 0, 8, 16, 32 and 64 h, in order to accelerate the corrosion. Behavior of the corrosion process was evaluated by means of electrochemical measurements using the Electrochemical Impedance Spectroscopy technique (EIS). The results showed an impedance reduction in concrete after impressed current exposure in all tested formulations. Lower reaction rates were observed in specimens with 0 and 15 wt% of SCBA content after 64 hours of accelerated corrosion. The impedance spectra of the samples with 45 wt% of SCBA cntent were compared with an equivalent circuit model, where high corrosion damage was observed.

Keywords: Accelerated corrosion, Electrochemical Impedance Spectroscopy, sugar cane bagasse ash, impressed current, X-ray photoelectron spectroscopy.

Resumen

Se estudió el comportamiento a la corrosión en barras de acero de refuerzo G42 embebidas en muestras cilíndricas de concreto modificado con cenizas de bagazo de caña de azúcar (SCBA). El cemento Portland fue reemplazado parcialmente en proporciones de 0, 15, 30 y 45% en peso por SCBA. Las muestras se expusieron a un medio salino utilizando la técnica de corriente impresa durante 0, 8, 16, 32 y 64 h para acelerar la corrosión. El comportamiento del proceso de corrosión se evaluó mediante mediciones electroquímicas utilizando la técnica de espectroscopía de impedancia electroquímica (EIS). Los resultados mostraron una reducción de la impedancia en el concreto después de la exposición a la corriente impresa en todas las formulaciones probadas. Se observaron velocidades de reacción más bajas en muestras con 0 y 15% en peso de contenido de SCBA después de 64 horas de corrosión acelerada. Los espectros de impedancia de las muestras con 45% en peso de contenido de SCBA se compararon con un modelo de circuito equivalente, donde se observó un alto daño por corrosión.

Palabras clave: Corrosión acelerada, espectroscopía de impedancia electroquímica, ceniza de bagazo de caña de azúcar, corriente impresa, espectroscopía de fotoelectrones por rayos X.

1 Introduction

The corrosion of steel reinforcements is considered as the most common degradation phenomenon of reinforced concrete structures, due to the progressive diffusion of chloride ion and carbon dioxide (Balan-Ortiz *et al.*, 2017). An increase in volume of corrosion products at the steel-concrete interface causes expanding stresses within the cement matrix leading to its disruption. Some research projects have made efforts to address this problem, by incorporating different types of mineral additions to concrete, including the ashes from the incineration of biomass. Research on this topic dates back to the 1970's, in which the first mixtures were comprised of a combination of ordinary Portland cement and rice husk ash due to latter's high content of amorphous silica (SiO_2), has shown performance enhancement in mechanical properties when compared with control Portland cement-based specimens (Mehta, 1977).

* *Corresponding author. E-mail*: cesar.sedano@academicos.udg.mx
https://doi.org/10.24275/rmiq/Mat1651
ISSN:1665-2738, *issn-e*: 2395-8472

Table 1. Analysis of previous work in corrosion of Portland cement (PC)-SCBA concretes.

Author	SCBA size (μm)	Concrete composition (%)	Tests	Electrode arrangement	Accelerated corrosion technique	Corrosive media	Sample geometry
Ganesan, 2007	46	PC: 95-70, SCBA: 5-30	LPR-EIS	WE-Steel bar CE-Stainless steel RE-Saturated Calomel	Dry-wet cycles	3% NaCl	10 cm cubes
Maldonado-Bandala, 2011	< 75	PC: 100-80, SCBA: 0-20	LPR	WE-Steel bar CE-Steel bar RE-$Cu/CuSO_4$	Immersion	3.5% NaCl 3.5% $NaSO_4$	9x15x15 cm prisms
Horsakulthai, 2011	10 to 30	PC: 100-60, Bagasse-rice husk-wood ash 10-40	Chloride penetration	N/A	Impressed voltage	3% NaCl	12x20 cm Cylinders
Nuñez-Jaquez, 2012	--	PC: 80 SCBA 20	LPR	WE-Steel bar CE-Stainless steel RE -Standard Calomel	Dry-wet cycles	3.5% NaCl	7x7x10 cm prisms
Nasir Shafiq, 2014	45	PC: 95-50 SCBA:5-50	Chloride penetration	N/A	Immersion	4% NaCl	10 cm cubes

In recent years, biomass ashes from other agricultural wastes have been incorporated in concrete, including as coconut pith, sawdust, cork granules (Ramaswamy *et al*., 1983), wood (Wang *et al*., 2008), corncob, wheat straw, plane leaf (Binici *et al*., 2008), grasses (Bajare *et al*., 2012; Cordeiro & Sales, 2015), periwinkle shell, bamboo leaf (Umoh *et al*., 2013), banana leaves (Kanning, *et al*., 2014), barley husk (Khalil *et al*., 2014), corn stalk, wheat straw, sunflower stalk (Aksoğan *et al*., 2016) and sugar cane bagasse ashes (SCBA) (Cordeiro *et al*., 2012; Sales & Lima, 2010).

Sugarcane bagasse has been used for wastewater treatment of the oil industry (Almeida *et al*., 2019) and Pb (II) removal (Tejada-Tovar *et al*., 2020). Nevertheless, by absorbing the contaminants, this material is used for combustion. In general, SCBA are generated worldwide from the incineration of sugarcane fibers as fuel in boilers after crushing and juice extraction processes in sugar factories (Noa-Bolaño *et al*., 2019). The residual ashes of this process are classified as bottom and fly ashes and have been successfully used as mineral additions for concrete production. Positive effects have been reported in concrete with bottom SBCA, as these generally offer an adequate pozzolanic activity in combination with Portland cement, with the subsequent formation of additional hydration products that improve some properties. This activity is associated to the presence of amorphous SiO_2 and Al_2O_3 in relatively small-sized particles, which react with the calcium hydroxide ($Ca(OH)_2$) to form mostly calcium silicate hydrate (C-S-H), but also calcium aluminum hydrate and AFm phases (Payá *et al*., 2002; Cordeiro *et al*., 2008).

Few studies exist on the durability of SCBA-modified concrete regarding chlorine ion penetration and the corrosion behavior of embedded steel reinforcing bars are given in Table 1. In most of them, authors used prismatic and cylindrical specimens and have used different electrochemical measurement techniques to determine corrosion rate and other methods to accelerate the corrosion process. One of the common situations is to make brine solutions to simulate their behavior in marine environments (Balan-Ortiz *et al*., 2017). Ganesan & Rajagopal (2007) evaluated the corrosion of carbon steel in concrete containing up to 25 wt% of SCBA with an average particle size of 46 μm. 10-cm sized cubic specimens were exposed to alternate dry-wet cycles in a 3% NaCl solution for 18 months. For electrochemical measurements, linear polarization resistance (LPR) and electrochemical impedance spectroscopy (EIS) techniques were used, finding a reduction of corrosion rate and chloride penetration for concrete specimens with the replacement of 20 wt% of sugarcane bagasse ashes. Meanwhile, Maldonado-Bandala *et al*. (2011) used SCBA particles < 75 μm with replacement levels of 5, 10, 15 and 20 wt%. Prismatic specimens with 9 × 15 × 15 cm were

immersed in a 3.5% NaCl solution for 14 months, accompanied with LPR technique to calculate the corrosion rate. They found that concrete with 20 wt% of SCBA showed a current density i_{corr} value 50% lower than the control conventional concrete. Nuñez-Jaquez *et al*. (2012) used 7 × 7 × 10 cm prismatic specimens replacing 20 wt% of cement with SCBA. In order to accelerate the corrosion process, they subjected specimens to immersion and drying cycles in a 3.5% NaCl solution, finding corrosion rates 40% lower than those of the conventional concrete using the LPR technique. Horsakulthai *et al*. (2011) used the ashes from the co-incineration of 82.5% bagasse, 15% rice husk, and 2.5% chop wood from an energy recovery plant. The resulting combined biomass ash was used as partial Portland cement at 10 and 20 wt%. They exposed 10 cm diameter × 20 cm height cylindrical specimens to an accelerated corrosion test by impressed voltage (ACTIV) immersed in a 3% NaCl solution. The results showed a high strength activity index; after 91 days, mixes with 20% of the combined ash presented a compressive strength 30% higher than that of the control. Additionally, chloride ion penetration was found to be about 65% lower after 28 days and the embedded steel reinforcement exhibited a corrosion-induced mass loss 85% lower when compared with the control.

SCBA has received special attention in sugar-producing countries due to its serious environmental impact. In an effort to decrease the amount of material sent to landfill and to reduce the negative impact of the cement industry, efforts have been carried out on the use of incinerated agricultural wastes as supplementary cementitious materials. Nevertheless, due to the limited use of SCBA as cementitious material, information of its effect as partial replacement of Portland cement in concrete is not extensively documented despite its proven pozzolanicity. Therefore, this work aims at studying the corrosion process of G42 steel reinforcement bars embedded in concrete with SCBA as cement substitute. This study examines the effect of mill scale on the intensity of the early stage corrosion process of specimens exposed to an aggressive saline environment that potentiate both carbonation and corrosion attack, using the ACTIV and EIS techniques.

2 Materials and methods

2.1 Materials

Portland cement CPC 30R Type I provided by "Cementos Tolteca" was used. The Portland cement has a density of 2.98 g·cm^{-3} and a Blaine specific surface area of 3960 cm^2·g^{-1}. Other properties are reported in Table 2. The SCBA was obtained from sugar factory"Ingenio José María Morelos" in Jalisco, Mexico. The boiler bottom ash was sieved in a no. 270 mesh (53 μm) and subsequently ground to reach an average particle size of 32 μm (Figure 1).

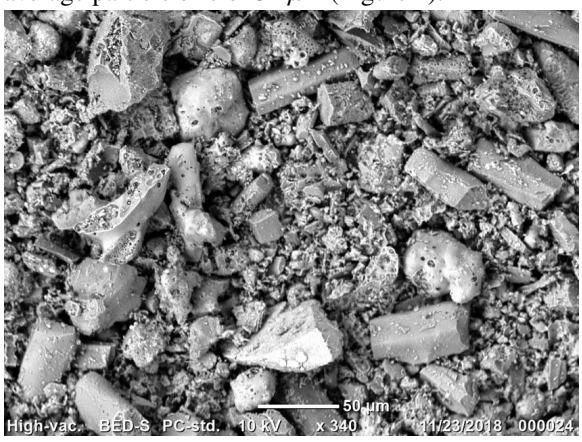

Fig. 1. Backscattered electron micrograph of SCBA after 2.5 h of milling.

Table 2. Portland cement properties.

Properties	NMX-C-414-ONNCCE	Test result
Blaine specific surface area	-	3960 cm^2/g
Expansion	< 0.8%	0.02%
Shrinking	< 0.2%	-
Vicat setting time	45 min - 600 min	200 min - 370 min
Density	-	2.985 g/cm^3
Volumetric weight	-	1240 kg/m^3
Expansion by sulfate attack during 1 year	< 0.1%	0.08%
SO_3	< 4.0%	2.9%

Table 3. Elemental composition (%) of SCBA by XPS technique.

C	O	K	Mg	Ca	Si	Fe	P	Al
10.2	42.2	1.6	9.0	1.3	17.9	0.4	1.5	15.0

Table 4. Physical properties of the silica sand.

Property	Value
Specific gravity (kg·m^{-3})	2590
Unit weight (kg·m^{-3})	1223
Water absorption (%)	0.95
Fineness modulus (FM)	1.99
Organic matter content (%)	0.5

The elemental composition, presented in Table 3, was performed by means of X-ray photoelectron spectroscopy technique (XPS).

Silica sand was used as the fine aggregate and 19-sized crushed stone as the coarse aggregate. The specific gravity in saturated surface-dry state for fine aggregate was 2590 kg/m^3. Other properties of the fine aggregates are presented in Table 4. Gradation curve of sand was compared with the regulation limits of ASTM C33 Standard Specification for Concrete Aggregates (ASTM Standard C33, 2003).

Grade 42 corrugated 12.7-mm sized carbon-steel bars, provided by "Compañía Siderúrgica Guadalajara", complying with the requirements of standard ASTM A615/615M-18 (2019), were used for the experimental work. The carbon steel rebar exhibited a fluency effort of 42 kg/mm^2, and a strain resistance of 63 kg/mm^2, meeting the Mexican standard NMX-B-506-CANACERO-2011. The bars were cleaned with acetone, keeping the mill scale on its surface before placement into the concrete specimens. An area of 75 cm^2 was left exposed and the rest coated with an insulating epoxy resin at room temperature.

2.2 *Methods*

The Portland cement was partially replaced with SCBA at the dosage of 15, 30 and 45 wt%. The results were compared against samples without SCBA. The compositions of concrete mixes are given in Table 5.

The test specimens consisted of 150 mm in diameter and 300 mm height reinforced concrete cylinders (standard ASTM C39/39M-2017 (2017)). A corrugated steel bar with a length of 300 mm was embedded 250 mm into the concrete specimen at the center of each cylinder acting as the working electrode. Likewise, a graphite bar of 6.4 mm in diameter was embedded placed 50 mm from the rebar, and worked as the reference electrode. The test specimen configuration is detailed in Figure 2.

Table 5. Mix design for 1 m^3 of concrete (kg).

Mix	Cement	SCBA	Sand	Coarse agg.	Water
0 SCBA	273	0	550	748	221
15 SCBA	232	41	550	748	221
30 SCBA	191	82	550	748	221
45 SCBA	150	123	550	748	221

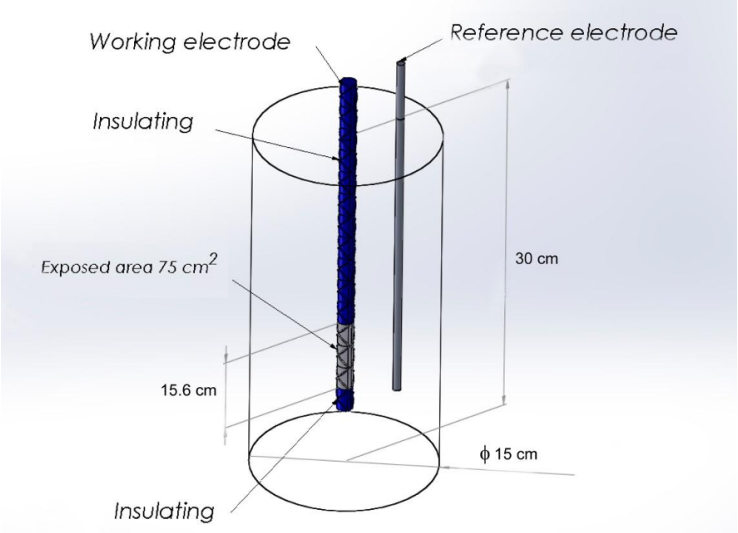

Fig. 2. Schematic diagram of cylindrical specimens.

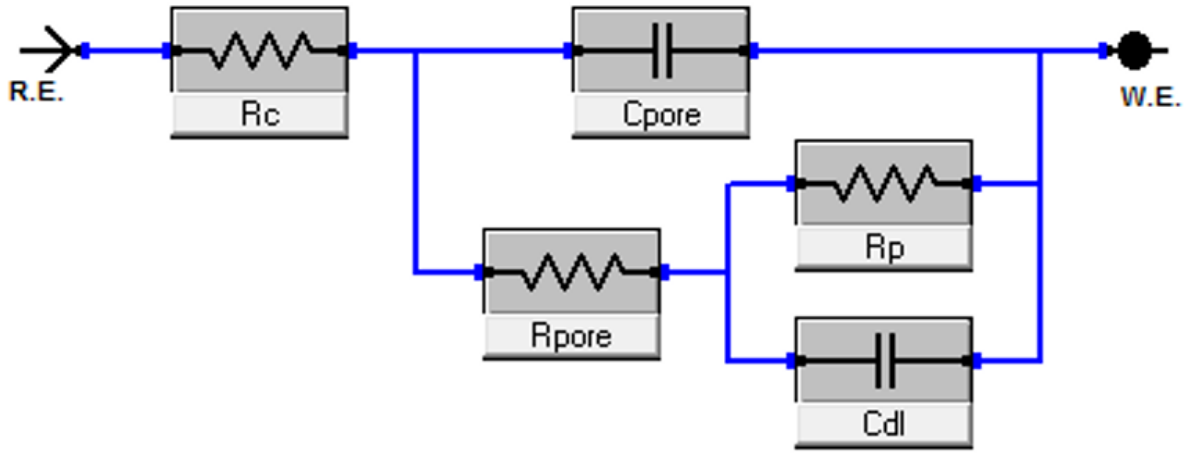

Fig. 3. Equivalent electrical circuit model that describes the corrosion behaviour of rebar-modified concrete interface

2.2.1 *Curing and exposure conditions*

After casting, the concrete specimens were kept in their molds at room temperature (23 ± 3 °C) for 24 h. They were then demolded and kept under the same conditions for 28 days. Afterwards, the specimens were partially immersed in a solution composed by deionized water and 25 g/L of NaCl and saturated by bubbling CO_2 at 69 kPa during 60 minutes to reduce the pH from 6.4 to 5.2. 2.5 cm were left exposed to atmosphere for 2 days to obtain uniform moisture distribution in the immersed part of the specimen. After this period, the specimens were subjected to accelerated corrosion testing.

2.2.2 *Methods of testing*

In order to evaluate the corrosion characteristics in terms of the initial current of reinforced concrete into corrosive media, accelerated corrosion test was performed attending some parameters of NT BUILD 356 method (1989). A potential of 7.9 ± 0.08 V of direct current was applied across the specimens. After immersion, the specimens' rebar was connected in parallel to the positive terminal of the source acting as the anode. A 900 cm^2 stainless steel flat bar arrangement connected to the negative terminal of the source served as cathode. The anodic current was recorded at increasing exposure times at cycles of 8, 16, 32 and 64 h. Specimens were drained for 24 h before the electrochemical measurements. Electrochemical impedance spectroscopy measurements were performed by means of a Gamry potentiostat model 1010E, from 100 kHz to 10 mHz at 10 mV, in accordance with standard ASTM G106-89 (2010). Electrochemical impedance data were collected to plot the Bode and Phase angle diagrams with respect to frequency. An equivalent electrical circuit model proposed by Mansfled & Kendig (1983) was used to simulate the corrosion phenomenon in the corrugated steel and modified concrete interface, which consists of a series-parallel arrangement of two capacitors and three resistors, as shown in Figure 3. Equation 1 describes the total impedance of the equivalent electrical circuit model shown in Figure 3.

$$Z = R_c + \frac{R_{pore}R_p + j\omega R_{pore}R_pC_{dl}}{1 + j\omega R_p(C_{dl} + C_{pore}) + j\omega R_{pore}C_{pore} + (j\omega)^2 R_{pore}C_{pore}C_{dl}} \quad (1)$$

where, Z is the impedance (ohms), R_c, R_{pore} and R_p are concrete, pore and interface resistances (ohms) respectively, C_{dl} and C_{pore} are the double layer and pore capacitances (Farads), ω is the angular frequency (rad/s) and j is the imaginary part of the impedance.

2.2.3 Experimental procedure

The samples were subjected to impressed current at 8, 16, 32 and 64 h to obtain accelerated rebar corrosion. In each case, three specimens were tested, and average values were reported. Open circuit potential (OCP) and EIS measurements were carried out to obtain the corrosion rate of specimens in different conditions. Impedance measurements were carried out with amplitude of 10 mV of alternating current. The impedance and phase angle were measured for the frequency range of 100 kHz - 10 mHz according to standard ASTM G106-89 (2010). A two-electrode setup was used, where the counter electrode terminal was short circuited with the reference electrode; the steel rebar embedded at the center was employed as working electrode, and the graphite bar was used as reference electrode due to its excellent conductivity and stability to pH changes (Poursaee, 2009; Muralidharan *et al*., 2006). The impedance data were displayed in Bode plot. All potentials in this study were referred to graphite electrodes. The corrosion potential of uncoated reinforcing steel embedded in concrete was measured according to standard test method ASTM C876-15 (2015). Before each measurement, the specimens were pre-wetted and drained during 24 h to decrease the electrical resistance of the system.

The corrosion potential provides a suitable estimation of the rebar corrosion state in concrete and shows the probability of corrosion. Carbonation products were characterized by means of JEOL Scanning Electron Microscope model JCM-6000 (SEM) and SPECS X-ray Photoelectron Spectroscope consisted of an XR 50 M monochromatic AlKα (h_v=1468.7 eV) X-ray source and Phoibos 150 spectrometer with one dimensional detector 1D-DLD provided by SPECS (Berlin, Germany). Corrosion products were analyzed by means of a PANalytical X-ray Diffractometer model Empyrean and SEM technique.

3 Results and discussion

3.1 Electrochemical measurements

OCP deviation with respect to the exposure time between steel rebar and graphite electrode is shown in Figure 4. Each point into the plot represents the average value of three measurements. All specimens exhibited a raise in corrosion activity with respect to the increment of exposure time. At an early stage, specimens with 45% of SCBA show less corrosion activity than other formulations. Nevertheless, after 32 h, this behavior changes showing an increment in corrosion activity. On the other hand, the 30% SCBA-containing mixes and control specimens showed a high probability of corrosion activity. Samples with 15% of SCBA showed greater stability to corrosion activity than other formulations after 64 hours of exposure. The obtained values are consistent with those presented by Ganesan and Rajagopal (2007), they reported lower and higher corrosion activity values than the control specimen for 15 and 30 wt% SCBA formulations, respectively. In addition, they used a saturated calomel electrode as a reference electrode attached to the concrete specimen using a wet sponge. Furthermore, Nuñez-Jaquez *et al*. (2012) present results for specimens with 20 wt% SCBA with less corrosive activity than control specimens. They also report the use of a saturated calomel electrode as a reference electrode. On the contrary, Maldonado-Bandala *et al*. (2011) report data for specimens with 15% SCBA with higher corrosive activity than control specimens. In their research, they use a Cu/$CuSO_4$ electrode as reference electrode. The data obtained in this study are within the region of 90% probability of corrosion, indicating a more active system than those presented in previous works. This can be attributed to the incorporation of the graphite electrode into the concrete specimen, showing better interaction within the system, and, on the other hand, considering the difference in potential between the saturated calomel and Cu/$CuSO_4$ electrodes, the graphite electrode has shown better performance in reinforcing concrete-steel systems (Duarte *et al*., 2014).

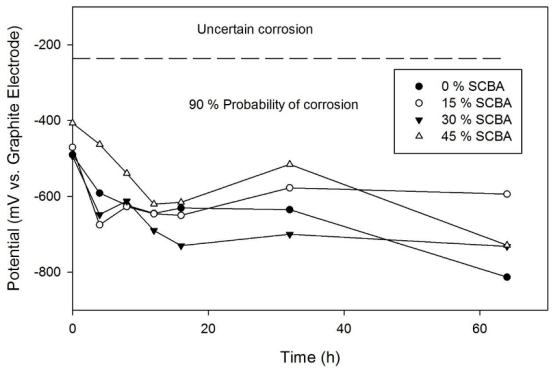

Fig. 4. Open circuit potential of reinforced bar vs. graphite electrode.

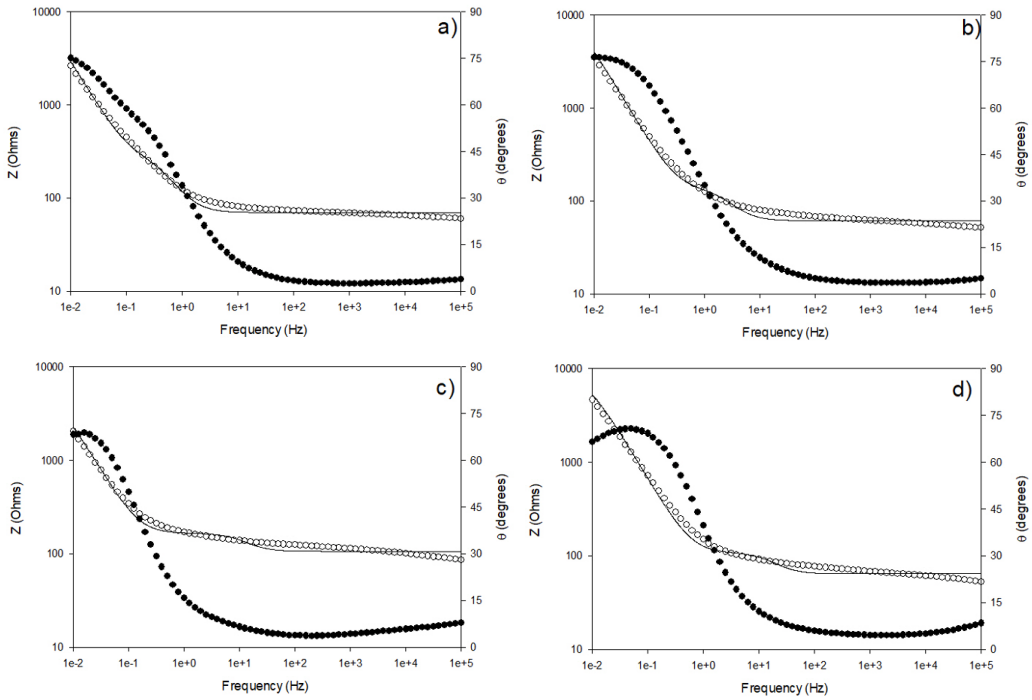

Fig. 5. Impedance spectra for concrete specimens without exposition of accelerated corrosion; a) 0% SCBA, b) 15% SCBA, c) 30% SCBA, d) 45% SCBA. Bode (○), phase angle (●), Equation 1 (___).

Experimental impedance spectra were obtained from EIS measurements for concrete specimens without exposure to accelerated corrosion, which are represented by Bode and phase angle plots, as seen in Figure 5. Bode diagrams relate the electrical resistance of concrete to high frequency domains. Furthermore, they provide the sum of all concrete-steel interface resistances at low frequency domains. Also, the phase angle graphs have been related to the porosity of some materials. Figure 5 shows that, at high frequency domains, most of the formulations exhibited impedance close to 65 Ω, except for samples with 30% of SCBA. Figure 5c shows 63% higher impedance than the other formulations, indicating a higher electrical resistivity and, consequently, a lower conductivity. At 10 mHz, the highest impedance of steel and concrete was of 4645 Ω for samples with 45% of SCBA. In addition, an impedance of 2626 Ω was measured for the control sample. This indicates that, before the impressed current, the control samples exhibited the lowest resistance to corrosion. On the other hand, in the phase angle plot it is possible to observe a displacement of the maximum value of the graph. Thus, as the content of SCBA increases, a peak displacement to a high frequency can be observed. This suggests that SCBA content affects the porosity of the system as shown by the results of Rukzon & Chindaprasirt (2012) and Sales & Lima (2010). A higher phase angle was observed for samples with 15% of SCBA. This indicates a greater capacitive response than the other formulations and, therefore, a lower corrosion rate would be expected for these samples. However, samples with 30% of SCBA showed the lowest phase angles, which indicates a lower capacitive response.

Figure 6 shows Bode and angle phase plots at 64 h of impressed current. At high frequency domains, most of the formulations exhibited impedance close to 45 *Omega*, which represents an impedance decrease of 31%. For samples with 45% SCBA, an impedance decrease of 62% with respect to 0 h was observed. On the other hand, the phase angle plots show a decrease in the peak value from 75° to 60° for specimens containing up to 30% SCBA. For specimens with 45% SCBA, the phase angle changed from 75° to 45°, indicating a reduction in the capacitance of the steel corrosion products/concrete interface. A double peak formation was observed with ash content increase, indicating the presence of two capacitive elements in the system described by the equivalent electrical circuit model (Figure 3) and Equation 1.

Table 6. Parameters of Equation 1.

Parameters	SCBA (%)	Time (h)				
		0	8	16	32	64
R_c (Ω)	0	70	52	50	44	51
	15	61	45	50	52	55
	30	106	58	50	48	46
	45	64	29	25	23	29
R_{pore} (Ω)	0	355	188	230	228	121
	15	108	64	39	31	43
	30	63	60	65	50	48
	45	51	40	38	39	50
R_p (Ω)	0	9984	10060	5017	3013	1128
	15	11510	10460	893	924	702
	30	4914	1593	1421	664	667
	45	8403	2549	651	598	210
C_{pore} (mF)	0	1.9	2.4	3.2	3.8	4.1
	15	0.9	1.0	1.9	2.3	4.8
	30	0.2	2.2	3.0	3.5	4.2
	45	0.2	1.0	1.4	2.6	5.2
C_{dl} (mF)	0	2.2	2.9	6.9	10.0	14.0
	15	2.9	3.3	24.0	21.0	29.0
	30	3.6	21.0	26.0	44.0	43.0
	45	6.3	21.5	22.0	50.0	70.0

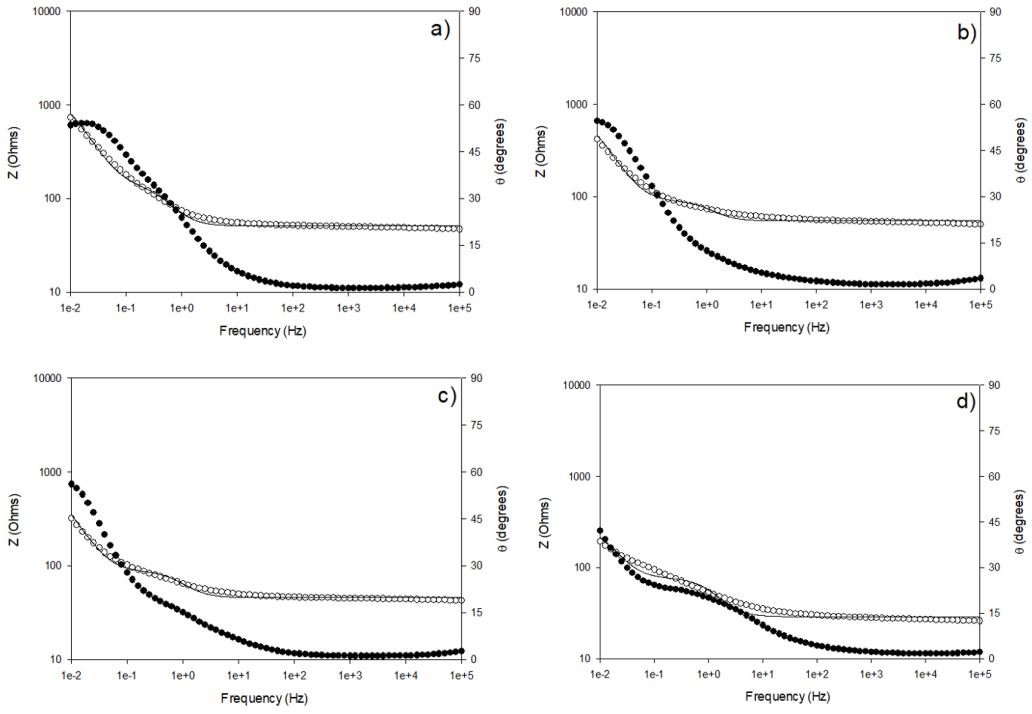

Fig. 6. Impedance spectra for concrete specimens with 64 h of accelerated corrosion exposure; a) 0% SCBA, b) 15% SCBA, c) 30% SCBA, d) 45% SCBA. Bode (○), phase angle (●), Equation 1 (___).

Parameters from Equation 1 are given in Table 6. R_p provides an indirect view of corrosion reaction at the steel-corrosion products interface. It is observed that raising the impressed current exposure time leads to a decrease of R_p values for all formulations, indicating an increased reaction of the steel-corrosion products interface with increasing immersion time in the saline solution. During the first 8 h of exposure, bubbling generated by the electrical activity of the corrosion products was observed at the steel-concrete interface, particularly more noticeable in the samples with 45% SCBA. The formulation with 15% SCBA had the highest R_p during the first 8 h; however, after 16 h of exposure, the R_p values decreased by 93% indicating an increase in the corrosion reaction. Formulation with 30% of SCBA maintained stable R_p values during the time of exposure to the impressed current. The 16-hour time is remarkable due to the possible partial removal of the mill scale from the steel rebar, promoting the arrival of species to be reduced on the surface of the mill scale, especially chloride ions that accelerate the corrosion reaction. R_{pore} is the resistance of the pore caused by the penetration of the electrolyte through generated corrosion products. For ash concentrations below 15%, a marked decrease in resistance caused by the porosity of corrosion products can be observed over time. For concentrations above 15% SCBA, there is no change in resistance caused by porosity. This can be attributed to the increase in the thickness of the corrosion layer promoted by the dissolution of the metal surface (Shi & Ming, 2017).

3.2 *Accelerated corrosion tests*

In accelerated corrosion tests, the anodic current was monitored from each specimen and plotted in Figure 7. The accelerated corrosion system showed high reaction activity during the first 8 h in all formulations, accompanied by a bubbling of corrosion products in the steel-concrete interface, being more noticeable for samples with 45% SCBA. After 8 hours, there is a slight reduction in the current associated with a loss of moisture from the corrosion products. A remarkable increase of 50% in circuit current from 280 mA to above 430 mA at 18 h of exposure time was noticed, especially for specimens with 45% SCBA. This behavior can be attributed to the degradation of the mill scale layer leaving the rebar surface vulnerable and to the high porosity observed in mixes with 45% SCBA. For other formulations, no significant change in the anode current of the circuit was perceived.

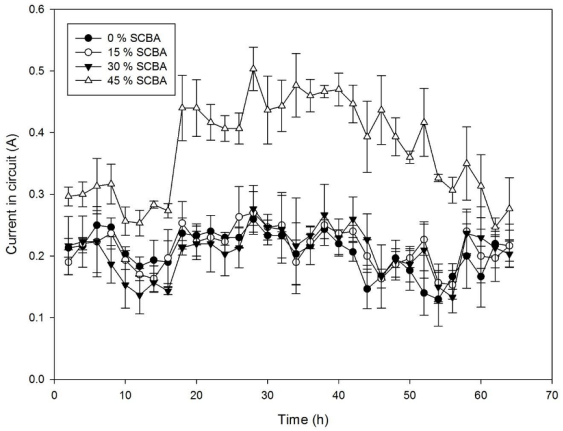

Fig. 7. Corrosion rate against time plot for modified concrete specimens.

However, these results are in disagreement with those of Horsakulthai *et al*. (2011) where, with an increasing replacement level of ashes up to 40%, the resistance to corrosion decreased by over 75% when compared to the control concrete. This could be attributed to those ashes' relatively small particle size and high SiO_2 content, which allow faster reaction resulting in less porosity and more products of hydration in an early age capable of physically and chemically binding the chloride ions. Naturally, these features retard the corrosion onset of the steel.

3.3 *Characterization of corrosion and carbonation products*

Cross-section cuts of the specimens were made after the electrochemical tests to characterize the corrosion products. These showed that mixes with 15% SCBA presented the lowest amount of corrosion products surrounding the reinforcing steel. The highest amount of corrosion products was found for 45% SCBA mixes. Figure 8 shows a SEM image of a steel-concrete interface observed in the sample after 64 h of accelerated corrosion embedded in a 45% SCBA concrete mix. The micrograph exhibits a common distribution of corrosion products at the steel-concrete interface. Four regions can be seen throughout the sample: expansive corrosion products; mill scale; corrosion products under the mill scale; and steel. Since the mill scale of a reinforcement bar embedded in concrete is porous (Jaffer & Hansson, 2009), it allows soluble species involved in the reaction to move through it, from the anodic to cathodic regions or in the opposite direction. It should be noted that chloride ions participate in the formation of these different layers.

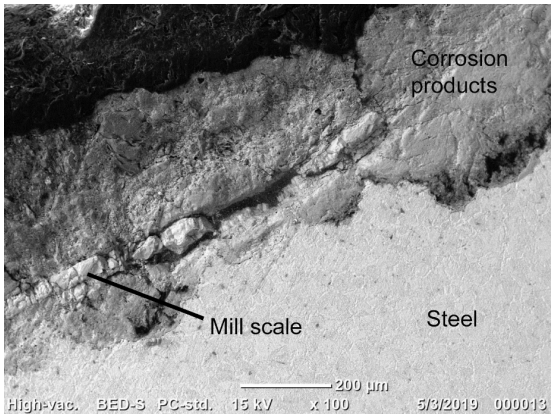

Fig. 8. Micrograph of the cross section of the corrugated steel bar after 64 h of accelerated corrosion and 45% of SCBA.

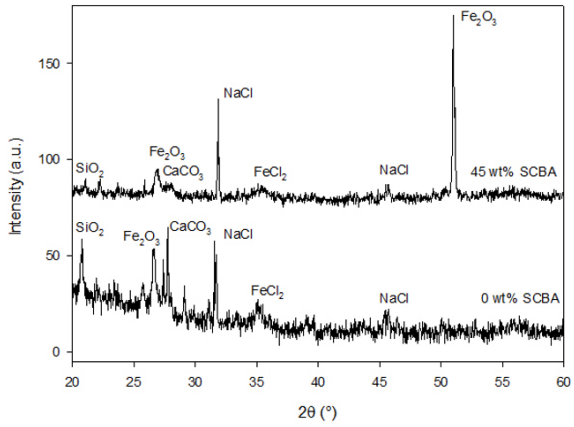

Fig. 9. XRD spectra of corrosion products after 64 h of accelerated corrosion for 0 and 45% SCBA.

$FeCl_2$ can be seen in the XRD spectrum presented in Figure 9. In CO_2-containing environments, carbonation of $Ca(OH)_2$ can occur, leading to the formation of $CaCO_3$ (28º in Figure 9). The mill scale was preserved after the growth of the corrosion layer because the iron (Fe) in the steel oxidizes more easily than that in iron oxides of the mill scale at low oxygen conditions. Fe_2O_3 formation is exhibited in the XRD spectrum at a 2θ angle of 52º. Addition of SCBA promoted the formation of Fe_2O_3 during the test, the peaks found at 26.5° and 51° at 2θ angle increase with iron oxide formation, and the relative height of the peaks compared with $CaCO_3$ seems to indicate a decrease in this compound. The carbonation products were taken from the upper edge of the cylindrical sample, approximately 7 cm from the steel rebar and, therefore, these products were not in direct contact with the corrosion products.

Figure 10 displays carbonation products after 32 h of impressed current, (a) without SCBA and (b) with 45% SCBA. In the latter, carbonation products show cubic crystalline formations. However, carbonation products of the control specimens exhibit amorphous formations. Figure 11 shows the XPS spectra for these types of carbonation products, which contain sodium carbonate as the main product. Although there is also the presence of $CaCO_3$ in a lower proportion. The XPS spectrum inferred the presence of NaCl in the carbonation products, which migrated from the brine solution, these results are consistent with Payá *et al*. (2002) and Cordeiro *et al*. (2008). The partial replacement of cement with SCBA suggests a relatively strong Ca spectrum, probably derived from $CaCO_3$, but also from other Ca-bearing phases (e.g. $Ca(OH)_2$, CaO, $CaCl_2$). In spite of the relatively lower intensity, the control sample also presents this spectrum.

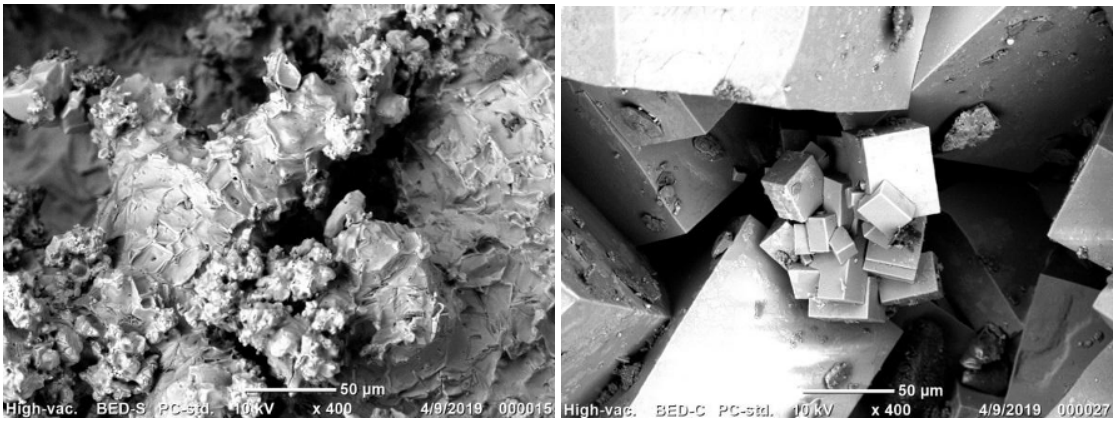

Fig. 10. Micrograph of electron backscattered carbonate formations on specimens with: a) 0% and b) 45% of SCBA after 32 h of impressed current.

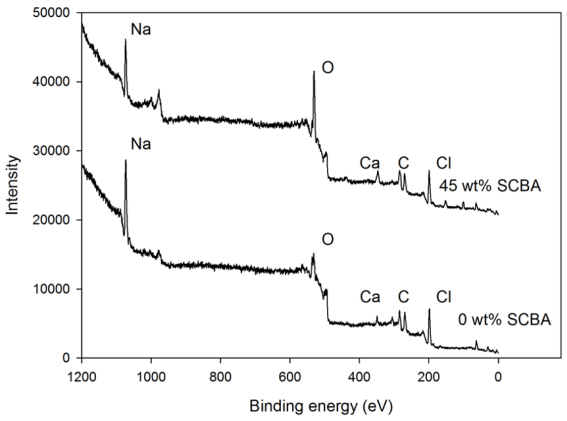

Fig. 11. XPS spectra of carbonation products of specimens with 0 and 45% SCBA after 32 h of impressed current.

Conclusions

Based on the results of the experimental investigation, the following conclusions were drawn: Graphite electrode into the concrete specimen shows better interaction within this kind of systems than other reported in literature; A reduction in concrete impedance was observed after exposure to the impressed current in all SCBA-containing formulations; Lower reaction rates were observed in specimens with 0 and 15% of SCBA content and 64 hours of accelerated corrosion; According to the cross-sections of specimens, a lower amount of corrosion products was noted on the rebar surroundings of control mixes and with 15% SCBA.

Acknowledgements

The authors wish to express their sincere appreciation to the PRODEP-SEP for financing part of this research work.

References

Aksoğan, O., Binici, H., & Ortlek, E. (2016). Durability of concrete made by partial replacement of fine aggregate by colemanite and barite and cement by ashes of corn stalk, wheat straw and sunflower stalk ashes. *Construction and Building Materials 106*, 253-263. https://doi.org/10.1016/J.CONBUILDMAT.2015.12.102

Almeida, F. B. P. S., Meili, L., Soletti, J. I., Esquerre, K. P. S. O. R., Ribeiro, L. M. O., & de Farias Silva, C. E. (2019). Oil produced water treatment using sugarcane solid residue as biosorbent. *Revista Mexicana de Ingeniería Química 18*, 27-38.

Bajare, D., Bumanis, G., Shakhmenko, G., and Justs, J. (2012). High performance and conventional concrete properties affected by ashes obtained from different type of grasses. *American Concrete Institute 289*, 1-14. Retrieved from https://www.concrete.org/publications/internationalconcreteabstractsportal/m/details/id/51684272

Balan-Ortiz, C. A., Luna Brito, M., Pérez López, T., & Camacho-Chab, R. J. (2017). Statistical analysis of electrochemical noise records obtained from the process of corrosion of reinforced steel embedded in concrete. *Revista Mexicana de Ingeniería Química 16*, 291-303.

Binici, H., Yucegok, F., Aksogan, O., & Kaplan, H. (2008). Effect of corncob, wheat straw , and plane leaf ashes. *Journal Of Materials In Civil Engineering 20*, 478-483. https://doi.org/10.1061/(ASCE)0899-1561(2008)20

BUILD, N. T. 356 (Approved 1989-11). Concrete, repairing materials and protective coating: embedded steel method, chloride permeability. *Nordtest* (Vol. 356, pp. 0-2).

Cordeiro, G.C., Toledo Filho, R. D., Tavares, L. M., & Fairbairn, E. M. R. (2012). Experimental characterization of binary and ternary blended-cement concretes containing ultrafine residual rice husk and sugar cane bagasse ashes. *Construction and Building Materials 29*, 641-646. https://doi.org/10.1016/J.CONBUILDMAT.2011.08.095

Cordeiro, G C, Filho, R. D. T., Tavares, L. M., & Fairbairn, E. M. R. (2008). Pozzolanic activity and filler effect of sugar cane bagasse ash in Portland cement and lime mortars. *Cement & Concrete Composites 30*, 410-418. https://doi.org/10.1016/j.cemconcomp.2008.01.001

Cordeiro, Guilherme Chagas, & Sales, C. P. (2015). Cement & concrete composites pozzolanic activity of elephant grass ash and its influence on the mechanical properties of concrete. *Cement And Concrete Composites 55*, 331-336. https://doi.org/10.1016/j.cemconcomp.2014.09.019

Duarte, R. G., Castela, A. S., Neves, R., Freire, L., & Montemor, M. F. (2014). Corrosion behavior of stainless steel rebars embedded in concrete: an electrochemical impedance spectroscopy study. *Electrochimica Acta 124*, 218-224.

Ganesan, K., & Rajagopal, K. (2007). Evaluation of bagasse ash as corrosion resisting admixture for carbon steel in concrete. *Anti-Corrosion Methods and Materials 54*, 230-236. https://doi.org/10.1108/00035590710762375

Horsakulthai, V., Phiuvanna, S., & Kaenbud, W. (2011). Investigation on the corrosion resistance of bagasse-rice husk-wood ash blended cement concrete by impressed voltage. *Construction and building materials 25*, 54-60. https://doi.org/10.1016/j.conbuildmat.2010.06.057

Jaffer, S. J., & Hansson, C. M. (2009). Chloride-induced corrosion products of steel in cracked-concrete subjected to different loading conditions. *Cement and Concrete Research 39*, 116-125. https://doi.org/10.1016/j.cemconres.2008.11.001

Kanning, R.C., Portella, F., Bragança, M. O. G. P., Bonato, M. M., & dos Santos, J. C. M. (2014). Banana leaves ashes as pozzolan for concrete and mortar of Portland. *Construction and Building Materials 54*, 460-465. https://doi.org/http://dx.doi.org/10.1016/j.conbuildmat.2013.12.030

Khalil, N. M., Hassan, E. M., Shakdofa, M. M. E., & Farahat, M. (2014). Beneficiation of the huge waste quantities of barley and rice husks as well as coal fly ashes as additives for Portland cement. *Journal of Industrial and Engineering Chemistry*. https://doi.org/10.1016/j.jiec.2013.11.034

Maldonado-Bandala, E. E., Jiménez-Quero, V. ., Olguin-Coca, F. J., Lizarraga, M., Baltazar-Zamora, M. A., Ortiz, A., ... Gaona-Tiburcio, C. (2011). Electrochemical characterization of modified concretes with sugar cane bagasse ash. *International Journal of Electrochemical Science 6*, 4915-4926.

Mansfled, F., & Kendig, M. K. (STP 866). (1983). Laboratory Corrosion Tests and Standards (STP 866) (ASTM Speci, Vol. 21; G. S. Haynes & I. Baboian, Robert. Texas Instruments, Eds. A.S.T.M.

Mehta, P. K. (1977). Properties of blended cements made from rice husk ash. *Journal Proceedings (American Concrete Institute)*, 440-442. Retrieved from https://www.concrete.org/publications/internationalconcreteabstractsportal/m/details/id/11022

Muralidharan, S., Ha, T.-H., Bae, J.-H., Ha, Y.-C., Lee, H.-G., Park, K.-W., & Kim, D.-K. (2006). Electrochemical studies on the solid embeddable reference sensors for corrosion monitoring in concrete structure. *Materials Letters 60*, 651-655. https://doi.org/10.1016/J.MATLET.2005.09.058

Noa-Bolaño, A., Pérez-Ones, O., Zumalacárregui-de Cárdenas, L., & Pérez-de-los-Ríos, J. L. (2020). Simulation of concentration and incineration as an alternative for vinasses' treatment. *Revista Mexicana de Ingeniería Química 19*, 1265-1275.

Núñez-Jaquez, R. E., Buelna-Rodríguez, J. E., Barrios-Durstewitz, C. P., Gaona-Tiburcio, C., & Almeraya-Calderón, F. (2012). Corrosion of modified concrete with sugar cane bagasse ash. *International Journal of Corrosion 2012*. https://doi.org/10.1155/2012/451864

Payá, J., Monzó, J., Borrachero, M. V, Díaz-Pinzón, L., & Ordónez, L. M. (2002). Sugar-cane bagasse ash (SCBA): Studies on its properties for reusing in concrete production. *Journal of Chemical Technology and Biotechnology 77*, 321-325. https://doi.org/10.1002/jctb.549

Poursaee, A. (2009). Automatic system for monitoring corrosion of steel in concrete. *Advances in Engineering Software 40*, 1179-1182. https://doi.org/10.1016/j.advengsoft.2009.05.001

Ramaswamy, S. D., Murthy, C. K., & Nagaraj, T. S. (1983). Use of waste materials and industrial by-products in concrete construction. *Concrete Technology and Design: New Concrete Materials 1*, 137-169.

Rukzon, S., & Chindaprasirt, P. (2012). Utilization of bagasse ash in high-strength concrete. *Journal Of Materials & Design 34*, 45-50. https://doi.org/10.1016/j.matdes.2011.07.045

Sales, A., & Lima, S. A. (2010). Use of Brazilian sugarcane bagasse ash in concrete as sand replacement. *Waste Management 30*, 1114-1122. https://doi.org/10.1016/j.wasman.2010.01.026

Shafiq, N., Elhsameed, A. A., & Nuruddin, M. F. (2014). Durability of Sugar Cane Bagasse Ash (SCBA) Concrete towards chloride ion penetration. In *Applied Mechanics and Materials* (Vol. 567, pp. 369-374). Trans Tech Publications Ltd. https://doi.org/10.4028/www.scientific.net/AMM.567.369

Shi, J. jie, & Ming, J. (2017). Influence of mill scale and rust layer on the corrosion resistance of low-alloy steel in simulated concrete pore solution. *International Journal of Minerals, Metallurgy and Materials 24*, 64-74. https://doi.org/10.1007/s12613-017-1379-4

Standard, A.S.T.M. A615/A615M-18 (2019), Standard specification for deformed and plain carbon-steel bars for concrete reinforcement. *Annual Book of ASTM Standards*. 1-8. https://doi.org/10.1520/A0615

Standard, A.S.T.M. C33 (2003), Standard specification for concrete Aggregates. *Annual Book of ASTM Standards*. 11. https://doi.org/10.1520/C0033

Standard, A.S.T.M. C876-15 (2020), Standard test method for corrosion potentials of uncoated reinforcing steel in concrete. *Annual Book of ASTM Standards*. 1-8. https://doi.org/10.1520/C0876-15.2

Standard, A.S.T.M.G106-89 (2019). Standard practice for verification of algorithm and equipment for electrochemical. *Annual Book of ASTM Standards* (Vol. 89). https://doi.org/10.1520/G0106-89R15.2

Tejada-Tovar, C., Mancilla, H. B., Moreyra, J. D. P., & Toro, R. O. (2020). Effect of the adsorbent dose in Pb (II) removal by using sugarcane bagasse: Kinetics and isotherms. *Revista Mexicana de Ingeniería Química 19*, 1413-1423.

Umoh, A. A., Olaniyi, A., Babafemi, A. J., & Femi, O. O. (2013). Assessing the mechanical performance of ternary blended cement concrete incorporating periwinkle shell and bamboo leaf ashes. *Civil and Environmental Research 3*, 26-36.

Wang, S., Miller, A., Llamazos, E., Fonseca, F., & Baxter, L. (2008). Biomass fly ash in concrete: Mixture proportioning and mechanical properties. *Fuel 87*, 365-371. https://doi.org/10.1016/j.fuel.2007.05.026